Correlation effects in p-electron magnets: the case of RbO$_2$

Roman Kováčik and Claude Ederer

School of Physics, Trinity College Dublin, Dublin 2, Ireland*

(Dated: May 22, 2009)

We present results of GGA+U calculations for the "d^0 magnet" RbO$_2$, where magnetic properties are due to partially filled oxygen p orbitals. We show that on-site interactions on the oxygen sites lead to a strong tendency towards the formation of an orbitally polarized insulating state, in contrast to the half-metallic behavior predicted for this class of compounds within pure LDA/GGA. The obtained energy differences between different orbitally ordered configurations are sizeable, indicating an orbital ordering temperature higher than the antiferromagnetic Néel temperature of ∼15 K. Our results demonstrate the importance of correlation effects in p electron magnets such as RbO$_2$.

Recently, various cases of "d^0-magnetism" have been reported where, in contrast to the more conventional case of partially filled d (or f) electronic shells, magnetic properties arise from partially filled p orbitals [1]. In most cases, the corresponding phenomena are defect-induced, and systematic studies are hampered by poor reproducibility and a wide spread in experimental data. Furthermore, theoretical investigations based on first principles density functional theory are plagued by the well-known deficiencies of the local spin-density and generalized gradient approximations (LDA and GGA) [2]. To further explore p electron magnetism as alternative option for spintronic applications, it is therefore desirable to study intrinsic p electron magnetism in pure, i.e. mostly defect-free, bulk materials, which can provide important insights in the underlying mechanisms and can serve as benchmarks for currently used theoretical approaches.

Here, we discuss the case of rubidium superoxide, RbO$_2$, which is part of the family of alkali-superoxides AO_2 (A = K, Rb, or Cs) [3, 4]. The magnetic properties of these systems result from the partially filled p electron levels of the superoxide anion O$_2^-$. As shown in Fig. 1a, the hybridization between atomic p orbitals within the O$_2$ units gives rise to bonding (σ_z, $\pi_{x,y}$) and anti-bonding (σ_z^*, $\pi_{x,y}^*$) molecular orbitals (MOs). The nine p electrons per O$_2^-$ occupy all bonding states, but leave one hole in the antibonding $\pi_{x,y}^*$ orbitals (see Fig. 1a), which can give rise to spin polarization and magnetic order (see Fig. 1b). Indeed, below the Néel temperature $T_N \sim 15$ K, RbO$_2$ orders antiferromagnetically, with parallel orientation of the magnetic moments within the tetragonal (001) planes and antiparallel orientation between adjacent planes [3, 4].

RbO$_2$ also undergoes several crystallographic phase transitions [4, 5], which involve various small distortions from an "average" high symmetry structure of the CaC$_2$-type (space group $I4/mmm$, see Fig. 1). This structure consists of two interpenetrating body-centered tetragonal lattices of Rb$^+$ cations and O$_2^-$ anions with the molecular O−O bond oriented parallel to the c axis. For simplicity, and since the full space group symmetries of the various low temperature phases have not been fully established, yet, all calculations presented in this work are performed
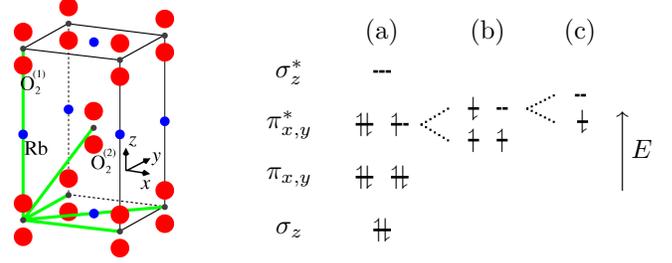

FIG. 1: (color online). Left: Averaged tetragonal structure of RbO$_2$. Oxygen and rubidium atoms are represented by large (red) and small (blue) spheres, respectively. In the following, the two O$_2$ molecules within the tetragonal unit cell will be denoted as O$_2^{(1)}$ and O$_2^{(2)}$. Thick solid (green) lines indicate the hoppings included in the TB model. Right: (a) Energy levels of O$_2^-$ molecules formed from atomic p states. (b) Spin polarization splits the majority and minority $\pi_{x,y}^*$ states. The degenerate half-filled minority-spin $\pi_{x,y}^*$ orbitals give rise to the half-metallicity obtained within LDA/GGA calculations. (c) An additional splitting results in an orbitally polarized insulating state consistent with experiment.

for the average CaC$_2$-structure shown in Fig 1.

In the following, we present results of first principles density functional theory calculations using the Quantum-ESPRESSO code package [6], employing the GGA exchange-correlation functional of Perdew, Burke, and Ernzerhof [7] and Vanderbilt ultrasoft pseudopotentials [8] (USPP). We analyze the effect of on-site Coulomb repulsion on the electronic structure of RbO$_2$ using the GGA+U approach [9, 10], and demonstrate that RbO$_2$ exhibits a strong tendency to form an orbitally polarized insulating state (see Fig. 1c), in contrast to the half-metallic character obtained within a simple LDA/GGA calculation. The orbital order occurs without imposing any symmetry-lowering of the crystal structure. Our results demonstrate the importance of correlation effects in p electron magnets such as RbO$_2$.

We start by performing a full structural optimization of RbO$_2$ within tetragonal $I4/mmm$ symmetry. These relaxations are done for antiparallel alignment of the magnetic moments of O$_2^{(1)}$ and O$_2^{(2)}$ (see Fig. 1). We use a plane wave cutoff energy of 30 Ry and a $10 \times 10 \times 6$
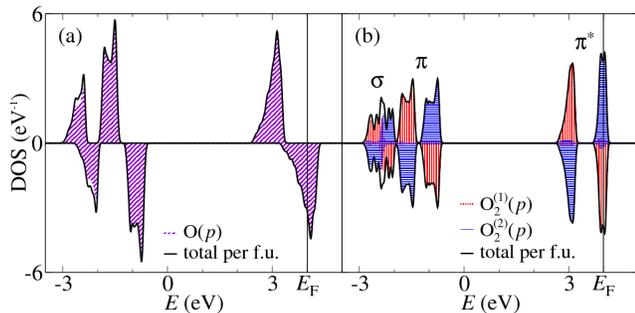
FIG. 2: (color online). DOS of RbO_2 for FM (a) and AFM (b) configuration. Black line represents total DOS; striped areas indicate $O(p)$ states (vertical: $O_2^{(1)}(p)$, horizontal: $O_2^{(2)}(p)$, diagonal: total $O(p)$). Different signs indicate different spin components.

FIG. 3: (color online). (a) Diagonal elements of the occupation matrix as a function of the Hubbard U parameter. (b) Evolution of the total DOS (black line) and projected DOS (vertical and horizontal stripes for $O(p_x)$ and $O(p_y)$, respectively) for different U values. The solid vertical line indicates the Fermi energy.

k-point grid, which result in convergence of the total energy better than 1 meV. We obtain lattice parameters $a = 4.20$ Å and $c = 7.07$ Å, in very good agreement with experimental values of 4.22 Å and 7.00 Å, respectively [5]. The calculated $O-O$ bond length is 1.36 Å which agrees very well with the experimental estimate of 1.34 Å [11].

The calculated densities of states (DOS) for both ferromagnetic (FM) and antiferromagnetic (AFM) configurations are shown in Fig. 2. It can be seen that in the plotted energy range around the Fermi level E_F the DOS has almost exclusive oxygen p character, and exhibits a peak structure closely resembling the molecular energy scheme depicted in Fig. 1. Thus, the relatively weak interaction between neighboring molecules leads only to a small broadening of the corresponding energy levels, i.e. the formation of very narrow bands that essentially retain the character of the corresponding MOs. The DOS for the two different magnetic configurations show only minor differences. In both cases, the Fermi level bisects the (local) minority $\pi^*_{x,y}$ band which leads to metallicity (half-metallicity for the FM case), similar to LDA calculations for KO_2 [12] and GGA calculations for rubidium sesquioxide, Rb_4O_6 [13, 14]. The latter material, which contains a mixture of superoxide and nonmagnetic peroxide anions, was predicted to be a half-metallic ferromagnet with an estimated Curie temperature of 302 K [13, 14]. However, experiments indicate that Rb_4O_6 is indeed a magnetically frustrated insulator exhibiting spin-glass-like behavior, consistent with more recent calculations using hybrid functionals and LDA+U [15, 16]. It was also pointed out in Ref. [15] that even RbO_2, which is experimentally well known to be an insulating antiferromagnet, is predicted to be half-metallic within LDA. This is consistent with our GGA calculations, which favor the FM over the AFM configurations by an energy difference of 6 meV per formula unit (f.u.), thus suggesting a general inadequacy of LDA/GGA for the treatment of partially filled molecular states.
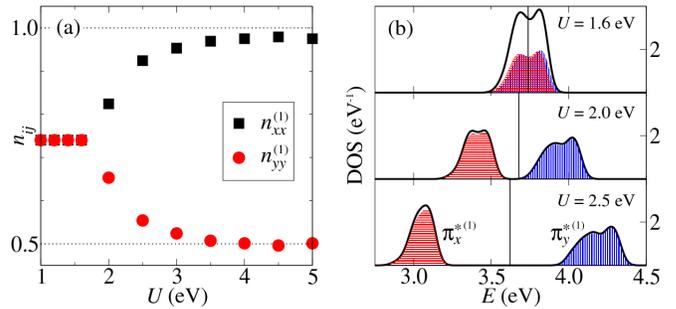
It is well known that LDA/GGA often fail to reproduce the correct insulating ground state for "strongly correlated" materials such as transition metal oxides and many f electron systems (see e.g. Ref. [10]). This failure can be corrected within the (LDA/GGA)+U method, by introducing a correction term accounting for strong on-site Coulomb interactions [9, 10]. For the implementation used in this work the corresponding energy correction has the form [17, 18]:

$$E_U = \frac{U}{2} \sum_{R,m,\sigma} \left(n_{mm}^{R\sigma} - \sum_{m'} n_{mm'}^{R\sigma} n_{m'm}^{R\sigma} \right) \quad . \quad (1)$$

Here, R, σ, and m indicate the site, spin, and orbital character, and the sum runs over all atoms/orbitals to which the Hubbard correction is applied. $n_{mm'}^{R\sigma}$ is the orbital occupation matrix obtained by projecting the occupied valence functions $|\psi_{\vec{k}\nu}^\sigma\rangle$ (ν: band index) onto atomic-like states $|\phi_m^R\rangle$:

$$n_{mm'}^{R\sigma} = \sum_{\vec{k},\nu} f_{\vec{k},\nu}^\sigma \langle \psi_{\vec{k}\nu}^\sigma | \phi_m^R \rangle \langle \phi_{m'}^R | \psi_{\vec{k}\nu}^\sigma \rangle \quad . \quad (2)$$

Here, $f_{\vec{k}\nu}^\sigma$ is the occupation of the corresponding wavefunction. In the following we suppress the superscript $R\sigma$ where possible; if not stated otherwise, occupation numbers refer to the local minority-spin p channel on the oxygen sites.

To assess the effect of on-site electron correlation for the present case of a partially filled p electron system we now perform a series of GGA+U calculations with varying Hubbard U parameter for the p orbitals on the oxygen sites. Within this scheme, an insulating state can in principle be achieved via orbital polarization, i.e. a preferred occupation of one of the degenerate π^* orbitals driven by correlation effects (see Fig. 1c). In the following we only consider the AFM configuration, and in order to allow
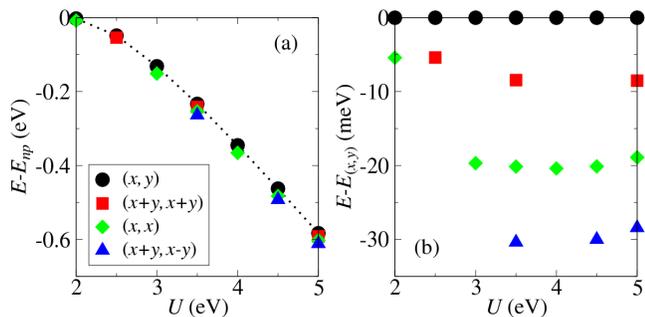
3

FIG. 4: (color online). (a) Total energy of orbitally polarized states relative to the non-polarized state as a function of U. (b) Energy of different orbitally ordered states relative to the (x, y) state. All energies correspond to the simple tetragonal unit cell.

FIG. 5: (color online). (a) Comparison of the band structure for π^* bands: GGA (thick/black line) and TB model (thin/red line). The two MLWF per O_2 site used as basis for the TB model are also shown. (b) Band gap as a function of U. Symbols for GGA+U data indicate the same orbital order patterns as in Fig. 4.

the system to converge to an orbitally polarized state, we initialize the elements of the orbital occupation matrix accordingly [19]. The resulting converged values of the occupation matrix elements as a function of U are summarized in Fig. 3a. Note that since the occupation matrix in the current GGA+U implementation refers to atomic $p_{x,y}$ states, which give rise to both the fully occupied bonding and the partially occupied antibonding MOs, a fully occupied π_x^* MO and fully unoccupied π_y^* MO correspond to atomic occupation numbers $n_{xx}=1.0$ and $n_{yy}=0.5$, whereas for the corresponding unpolarized state $n_{xx}=n_{yy}=0.75$. It can be seen from Fig. 3a that no orbital polarization develops for U values of up to 1.6 eV, while for $U=2.0$ eV a small occupation imbalance occurs. The orbital polarization increases with increasing U, and for $U>3.0$ eV the system is essentially fully polarized. The orbital polarization is accompanied by the opening of a gap in the DOS, and the system is fully insulating for $U>2.0$ eV (see Fig. 3b). The orbital polarization is also apparent from the projected DOS, indicating nearly exclusive p_x/p_y character in the occupied/unoccupied states, respectively.

Fig. 4a shows the energy gain due to orbital polarization for different orbital order patterns. The notation (a, b) indicates the orientation of the occupied orbitals on the two different O_2 units within the simple tetragonal unit cell, i.e. a/b can indicate occupation of either $\pi_{x,y}^*$ or $\left(\pi_x^* \pm \pi_y^*\right)/\sqrt{2}$ orbitals. All results presented so far refer to the (x, y)-type ordering, i.e. an anti-ferro-orbital ordering of occupied π_x^* and π_y^* orbitals. Convergence of the various orbital patterns can be achieved by varying the initialization of the orbital occupation matrix. As expected from Eq. (1), the calculated energy gain associated with orbital polarization (Fig. 4a) increases linearly with U for $U>3.0$ eV, where the system is essentially fully polarized. Fig. 4b shows the energies of the four different ordering patterns relative to the (x, y) type ordering [20]. The energy differences between the different cases are rather independent of U
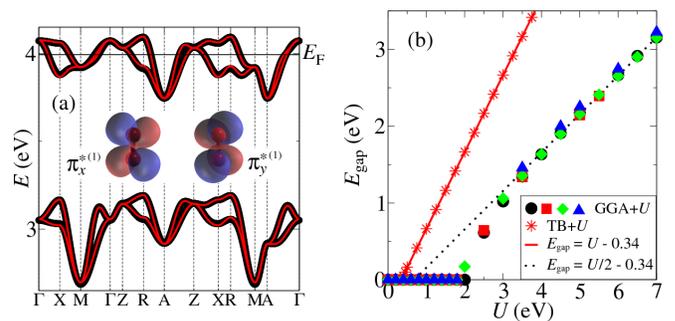
(for $U \geq 3.5$ eV) and are all of the order of $\sim$10 meV, with the diagonally-oriented anti-ferro-orbital ordering $(x+y, x-y)$ being energetically most favorable. The energy scale of $\sim$10 meV suggests a relatively high ordering temperature of $\sim$100 K. We point out that we do not consider any lattice distortion accompanying the orbital order so that these energy differences represent a purely electronic effect.

In order to gain further insight into the mechanism underlying the orbital ordering, we construct a minimal tight-binding (TB) model for the antibonding π^* MOs, similar to the one discussed in Ref. [12] for KO_2. In addition to the kinetic hopping term, we also include a mean-field Hubbard interaction resembling the "+U" correction term of the GGA+U approach (Eq. (1)). The hopping amplitudes are obtained by constructing maximally localized Wannier functions [21, 22] (MLWF) representing the antibonding $\pi_{x,y}^*$ states around the Fermi level. Hopping up to 4th nearest neighbors is considered in the TB model (indicated by thick solid/green lines in Fig. 1), leading to excellent agreement between the TB and GGA bands (see Fig. 5a). More details about the TB+U model will be presented elsewhere.

Within this TB+U model, we always obtain a polarization of the $(x \pm y, x \pm y)$-type, i.e. an orientation of the occupied π^* orbital along the diagonal in-plane direction. The corresponding ferro- and anti-ferro-orbital configurations are degenerate for the AFM case. Fig. 5b shows the evolution of the band gap as function of the Hubbard U for both the TB and the GGA+U calculations. Note that, as previously discussed, a full orbital polarization ($\Delta n \approx 1$) of the π^* MOs corresponds to an occupation difference $\Delta n \approx 0.5$ in the basis of atomic p orbitals used for the GGA+U calculations. Thus, the same on-site energy splitting $\Delta\epsilon = U\Delta n$ corresponds to twice the value of U in the GGA+U calculation compared to the TB model. Within the TB model a fully insulating state is obtained for $U \geq 0.5$ eV, where the width of
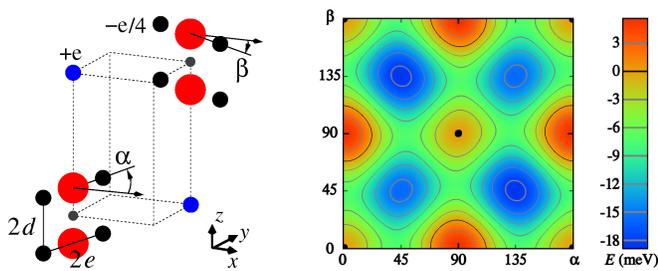
FIG. 6: (color online). Left: Point charge model for the electrostatic interaction. Occupied orbitals at each O_2^- unit are approximated by four $-e/4$ charges located at the positions of the MLWF extrema ($d = 0.68$ Å, $e = 0.42$ Å) and $+e$ charges are located at the Rb^+ sites. The orientations of the two occupied MOs are represented by angles α and β. Right: Corresponding electrostatic energy per unit cell as function of α and β.

the band-gap follows a linear relation $E_{\text{gap}}^{\text{TB}} = U - U_0$ with $U_0 = 0.34$ eV. The corresponding expectation for the GGA+U calculation is thus $\Delta E_{\text{gap}}^{\text{GGA}} = U/2 - U_0$. It can be seen from Fig. 5b that this relation is well fulfilled for $U > 3.5$ eV, where the system is indeed fully polarized (see Fig. 3a). The strong suppression of the orbital polarization for $U < 3.0$ eV in the GGA+U case indicates the importance of electrostatic effects which are not included in the TB+U model.

Full orbital polarization results in a pronounced asymmetry of the valence charge density, which is unfavorable from an electrostatic point of view. In order to assess the influence of this effect on the orbital order, we calculate the corresponding electrostatic energy contribution within a simple point charge model (see Fig. 6). It can be seen that the corresponding energy has pronounced minima at $\alpha, \beta = 45°$ or $135°$, corresponding to occupied $(\pi_x^* \pm \pi_y^*)/\sqrt{2}$ orbitals. The electrostatic interaction thus favors the same diagonal orientation of the occupied orbitals as the hoppings, and furthermore the degeneracy between the corresponding ferro- and anti-ferro-orbital orientation is lifted in favor of the $(x + y, x - y)$-type anti-ferro-orbital ordering ($\alpha = 45°$, $\beta = 135°$). This is also consistent with the result of the GGA+U calculations (Fig. 4b), even though the very simple point charge model is not able to fully account for the energetics between all the different configurations.

In summary, our calculations show that the p electron magnet RbO_2 exhibits a very strong tendency towards orbital polarization, driven by strong on-site interactions. An orbitally ordered insulating state appears for rather small values of the Hubbard U ($U_0 = 0.34$ eV for the MO basis). We note that $U \approx 3.55$ eV was determined in Ref. [12] for the molecular π^* orbitals in KO_2 based on constrained LDA calculations. The calculated energy differences between different orbital order patterns are of the order of 10 meV, and further analysis indicates that the orbital order pattern is determined by

both hybridization effects (hopping) and electrostatic interactions. While our study is limited by the rather small unit cell size used to explore different orbital order patterns, our results give clear evidence for the importance of correlation effects in p electron magnets. An interesting question that arises is how the correlation-induced orbital order discussed here affects the structural distortions via Jahn-Teller-like effects and elastic interactions. The same effects are likely to be important also for defect-related p electron magnetism, which means that simple LDA/GGA approaches cannot be used for reliable predictions of ordering temperatures and other characteristics in such systems.

———

* Electronic address: kovacikr@tcd.ie
[1] J. M. D. Coey, Solid State Sciences **7**, 660 (2005).
[2] A. Droghetti, C. D. Pemmaraju, and S. Sanvito, Phys. Rev. B **78**, 140404(R) (2008).
[3] A. Zumsteg, M. Ziegler, W. Känzig, and M. Bösch, Phys. Condens. Matter **17**, 267 (1974).
[4] M. Labhart, D. Raoux, W. Känzig, and M. A. Bösch, Phys. Rev. B **20**, 53 (1979).
[5] M. Rosenfeld, M. Ziegler, and W. Känzig, Helv. Phys. Acta **51**, 298 (1978).
[6] P. Giannozzi *et al.*, www.quantum-espresso.org.
[7] J. P. Perdew, K. Burke, and M. Ernzerhof, Phys. Rev. Lett. **77**, 3865 (1996).
[8] D. Vanderbilt, Phys. Rev. B **41**, 7892 (1990).
[9] V. I. Anisimov, J. Zaanen, and O. K. Andersen, Phys. Rev. B **44**, 943 (1991).
[10] V. I. Anisimov, F. Aryasetiawan, and A. I. Liechtenstein, J. Phys.: Condens. Matter **9**, 767 (1997).
[11] H. Seyeda and M. Jansen, J. Chem. Soc., Dalton Trans. pp. 875–876 (1998).
[12] I. V. Solovyev, New J. Phys. **10**, 013035 (2008).
[13] J. J. Attema, G. A. de Wijs, G. R. Blake, and R. A. de Groot, J. Am. Chem. Soc. **127**, 16325 (2005).
[14] J. J. Attema, G. A. de Wijs, and R. A. de Groot, J. Phys.: Condens. Matter **19**, 1 (2007).
[15] J. Winterlik, G. H. Fecher, and C. Felser, J. Am. Chem. Soc. **129**, 6990 (2007).
[16] J. Winterlik, G. H. Fecher, C. A. Jenkins, C. Felser, C. Mühle, K. Doll, M. Jansen, L. M. Sandratskii, and J. Kübler, Phys. Rev. Lett. **102**, 016401 (2009).
[17] S. L. Dudarev, G. A. Botton, S. Y. Savrasov, C. J. Humphreys, and A. P. Sutton, Phys. Rev. B **57**, 1505 (1998).
[18] M. Cococcioni and S. de Gironcoli, Phys. Rev. B **71**, 035105 (2005).
[19] Since the orbital polarization reduces the symmetry of the electronic structure from tetragonal to orthorhombic, it is essential to disregard all non-orthorhombic symmetry operations during the calculation. To achieve this, we simply neglect all symmetry operations and use the full

k-point mesh in all calculations.

[20] Note that due to restrictions in the way the orbital occupations can be initialized, we were not able to systematically converge all four patterns for all considered U values.

[21] N. Marzari and D. Vanderbilt, Phys. Rev. B **56**, 12847 (1997).

[22] I. Souza, N. Marzari, and D. Vanderbilt, Phys. Rev. B **65**, 035109 (2001).